2011

A Pt-Cluster-Based Heterogeneous Catalyst for Homogeneous Catalytic Reactions: X-ray Absorption Spectroscopy and Reaction Kinetic Studies of Their Activity and Stability against Leaching

Yimin Li, *University of California - Berkeley*
Jack Hung Chang Liu, *University of California - Berkeley*
Cole A. Witham, *University of California - Berkeley*
Wenyu Huang, *University of California - Berkeley*
Matthew A. Marcus, *University of California - Berkeley*, et al.

JACS
JOURNAL OF THE AMERICAN CHEMICAL SOCIETY

ARTICLE

pubs.acs.org/JACS

A Pt-Cluster-Based Heterogeneous Catalyst for Homogeneous Catalytic Reactions: X-ray Absorption Spectroscopy and Reaction Kinetic Studies of Their Activity and Stability against Leaching

Yimin Li,[†] Jack Hung-Chang Liu,[†] Cole A. Witham,[†] Wenyu Huang, Matthew A. Marcus, Sirine C. Fakra, Pinar Alayoglu, Zhongwei Zhu, Christopher M. Thompson, Arpana Arjun, Kihong Lee, Elad Gross, F. Dean Toste,* and Gabor A. Somorjai*

Department of Chemistry, University of California, Berkeley, California 94720, and United States Chemical and Materials Sciences Divisions and Advanced Light Source, Lawrence Berkeley National Laboratory, 1 Cyclotron Road, Berkeley, California 94720, United States

Supporting Information

ABSTRACT: The design and development of metal-cluster-based heterogeneous catalysts with high activity, selectivity, and stability under solution-phase reaction conditions will enable their applications as recyclable catalysts in large-scale fine chemicals production. To achieve these required catalytic properties, a heterogeneous catalyst must contain specific catalytically active species in high concentration, and the active species must be stabilized on a solid catalyst support under solution-phase reaction conditions. These requirements pose a great challenge for catalysis research to design metal-cluster-based catalysts for solution-phase catalytic processes. Here, we focus on a silica-supported, polymer-encapsulated Pt catalyst for an electrophilic hydroalkoxylation reaction in toluene, which exhibits superior selectivity and stability against leaching under mild reaction conditions. We unveil the key factors leading to the observed superior catalytic performance by combining X-ray absorption spectroscopy (XAS) and reaction kinetic studies. On the basis of the mechanistic understandings obtained in this work, we also provide useful guidelines for designing metal-cluster-based catalyst for a broader range of reactions in the solution phase.

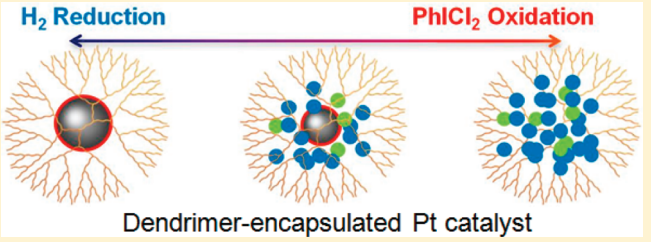

INTRODUCTION

At present, homogeneous catalytic processes dominate in industrial applications for fine chemicals production due to the high activity and selectivity associated with homogeneous catalysts. However, the lack of catalyst recyclability and the complicated catalyst removal process are major obstacles in improving the cost and energy efficiency of homogeneous catalytic processes.[1,2] Various approaches for heterogenization of homogeneous catalysts are currently under intensive research efforts, aiming at improving catalyst recyclability and facilitating product separation in fine chemicals production and in the pharmaceutical industry.[3−7]

As compared to single-metal-centered heterogenized homogeneous catalysts, metal-cluster-based catalysts have several unique advantages.[8] The synthesis of metal-cluster-based catalysts is relatively straightforward, which is more suitable for low-cost and large-quantity production for the industrial applications. Moreover, the existence of metal−metal bonding in metal clusters may lead to unique activity and selectivity not found in single-metal-centered homogeneous catalysts.[9,10] However, the concentrations of catalytically active species in metal-cluster-based catalysts are usually difficult to control, which makes it challenging to optimize catalytic activity and selectivity. Furthermore, because the metal atoms in the metal-cluster-based catalysts are not necessarily covalently bound to solid supports, the leaching of metal active species under liquid-phase reaction conditions is another important issue.[4,11]

In a recent publication, we reported on the catalytic performance of Pt_{40} G4OH/SBA-15, a silica-supported dendrimer-encapsulated Pt cluster <1 nm in size, for a series of solution-phase electrophilic π-bond activation reactions[12] that can be catalyzed homogeneously by $PtCl_2$ (see a reaction example in Scheme 1).[13,14] The Pt catalyst was activated by an oxidant, $PhICl_2$. It was found that this supported Pt catalyst exhibits high selectivity comparable to its homogeneous counterpart. More importantly, under typical reaction conditions at 100 °C in toluene, no leaching of catalytically active species into the solution was detected, and the catalyst was recyclable for multiple uses. More recently, an analogous Pd-based catalyst synthesized using this approach exhibited not only stability against leaching but also an exceptionally high activity for the same hydroalkoxylation reaction at room temperature, which exceeded that of most known homogeneous Pd-based catalysts under otherwise identical conditions.[15] The high activity and superior stability of this supported Pd catalyst made it possible to perform the reaction in a plug flow reactor, which is ideal for many applications in bulk-volume

Received: May 10, 2011
Published: July 01, 2011

Scheme 1. Hydroalkoxylation Reaction Catalyzed by a Silica-Supported and Dendrimer-Encapsulated Pt Catalyst (Pt_{40} G4OH/SBA-15)[a]

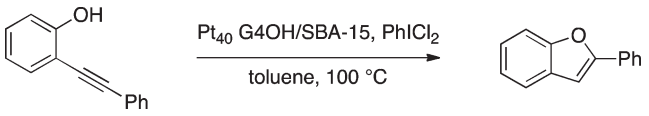

[a] In this reaction, the Pt clusters containing about 40 atoms are encapsulated in a dendrimer (PAMAM G4-OH) and supported on mesoporous silica (SBA-15). The oxidant, $PhICl_2$, is used to oxidize Pt into Pt chlorides, which serve as the electrophilic catalyst assisting the π-bond activation. Toluene is used as the solvent. The reaction temperature is 100 °C.

fine chemicals production. Despite the exciting progress in reaction studies of this metal-cluster catalyst, there are still fundamental issues that need to be addressed, such as the chemical composition, the stability of catalytically active species, and the mechanism by which leaching is inhibited. This critical mechanistic information will enable further optimization of catalytic activity and the development of highly stable metal cluster catalysts for a broader range of reactions in the solution phase.

In general, mechanistic investigation on the metal-cluster catalyzed solution-phase reaction has been experimentally challenging.[9,16] First, an activated metal-cluster catalyst may contain multiple species that may possess different catalytic activities under the reaction conditions.[17] Therefore, a technique capable of resolving and monitoring the multiple species coexisting in the catalyst under solution reaction environment must be used.[18] Second, the catalyst samples with varying relative concentrations of different species must be prepared so that comparative reaction kinetic studies can be performed to identify the catalytically active species.

In this article, we present mechanistic investigations on the Pt_{40} G4OH/SBA-15 catalyst for the electrophilic hydroalkoxylation reaction shown in Scheme 1. X-ray absorption spectroscopy (XAS), including extended X-ray absorption fine structure (EXAFS) and near-edge X-ray absorption fine structure (NEXAFS), were used to obtain the structural and composition information of the Pt catalysts. To establish the composition−activity correlation of the Pt catalyst, samples with varying degree of oxidation were prepared by a sequence of pretreatments including reduction by H_2 and oxidation by $PhICl_2$. XAS measurements showed that the catalysts activated by the $PhICl_2$ oxidation consist of metallic Pt(0) as well as Pt(II) and Pt(IV) chlorides. With the aid of reaction kinetic measurements, it was found that the conversion rate increases with the fraction of Pt(IV) chloride in the activated catalysts. The evolution of the fractions of Pt species in an activated catalyst was monitored by in situ NEXAFS under reaction conditions to elucidate the mechanism of the observed deactivation of the catalyst. On the basis of the XAS results, a leaching-inhibition mechanism related to the disparity of polarities between the toluene and the catalyst materials is proposed and verified by a series of control experiments.

RESULTS AND DISCUSSION

Structure and Chemical Composition of the Pt Catalysts. In homogeneous π-bond activation reactions, a well-defined electrophilic Pt complex with a known oxidation state can act as a catalytically active species.[13,14] In contrast, when the Pt cluster catalyst is used for the reaction, the $PhICl_2$ oxidation may generate multiple Pt chloride species that coexist in the dendrimer. Therefore, techniques such as XAS are needed to elucidate their structural and composition information under solution-phase reaction conditions.

To examine the structure and the degree of oxidation of the Pt catalyst, XAS measurements were performed on the catalyst samples, **Reduction 1**, **Reduction 2**, **Oxidation 1**, and **Oxidation 2**, prepared by a sequence of treatments, including reduction by hydrogen and oxidation by $PhICl_2$ (the details of the treatment procedure are given in the Experimental Section). Through EXAFS analysis at the Pt L_3 edge (Figure 1a), it is found that the Pt−Pt coordination number of the reduced Pt catalyst, **Reduction 1**, is about 5, which indicates the formation of reduced Pt clusters of about 1 nm in size.[19] After the oxidation treatment by $PhICl_2$, the Pt−Pt coordination numbers of the oxidized samples decreased to below 1, while the Pt−Cl coordination numbers increased. The changes in oxidation state of the catalyst are also reflected in the fractions of Pt(0), Pt(II), and Pt(IV) species obtained from NEXAFS analysis (Figure 1b). Figure 1a and b also shows that the structure of the Pt catalyst, in terms of Pt coordination numbers and the Pt oxidation state, is reversible during the sequence of reduction and oxidation treatment.

The pronounced change in the oxidation state of this Pt catalyst induced by pretreatment is a characteristic feature of monodispersed metal clusters of <1 nm in size. Within this cluster size range, most of the metal atoms are on the cluster surfaces and readily react with a reducing or oxidizing agent.[20,21] Therefore, the oxidation states of these small clusters can be more easily controlled by a pretreatment than that of larger clusters.

The EXAFS result in Figure 1a shows that the Pt−Pt coordination number of **Oxidation 1** is about 1. If all Pt species are uniform in structure, it is expected that a Pt dimer would be the dominant species in this sample. In this case, the Pt dimers ought to be oxidized by the oxidant presented in the solution to form complexes with rich Pt−Cl bonding. Thus, a very low fraction of Pt(0) species in this sample would be expected. On the contrary, the NEXAFS results shown in Figure 1b indicate that there is an unexpectedly high fraction (∼50%) of Pt(0) in the sample. To reconcile the EXAFS and NEXAFS results, it is proposed that the structure and oxidation state of Pt species in this sample are not uniform. Through the $PhICl_2$ oxidation, some of the clusters in the sample are disintegrated and are oxidized to Pt(II) and Pt(IV), while small Pt(0) clusters remain (Figure 1c).

Catalytically Active Species. In the reaction kinetics studies, conversion was measured as a function of reaction time in a batch reaction mode (see Experimental Section for details) and the rate constant calculated by fitting the conversion curve to the first-order kinetic model for a unimolecular reaction. In this way, the relative catalytic activity of each catalyst could be quantified by its rate constant; however, given the changing nature of the catalyst (see below), quantitative measurements of rate constants for given catalyst compositions were difficult to ascertain. Nevertheless, the reaction kinetics studies clearly show that **Oxidation 2** has a much higher catalytic activity than **Oxidation 1** (a 10-fold difference in the rate constant can be seen in Figure 1d), which correlates with the initially higher fraction of the Pt(IV) species in **Oxidation 2** (Figure 1b). Because Pt(IV) is more electrophilic than Pt(II), it is more active in this π-bond activation reaction, which is consistent with the observed higher activity of $PtCl_4$ in homogeneous π-bond activation reaction.[22] For **Oxidation 2**,

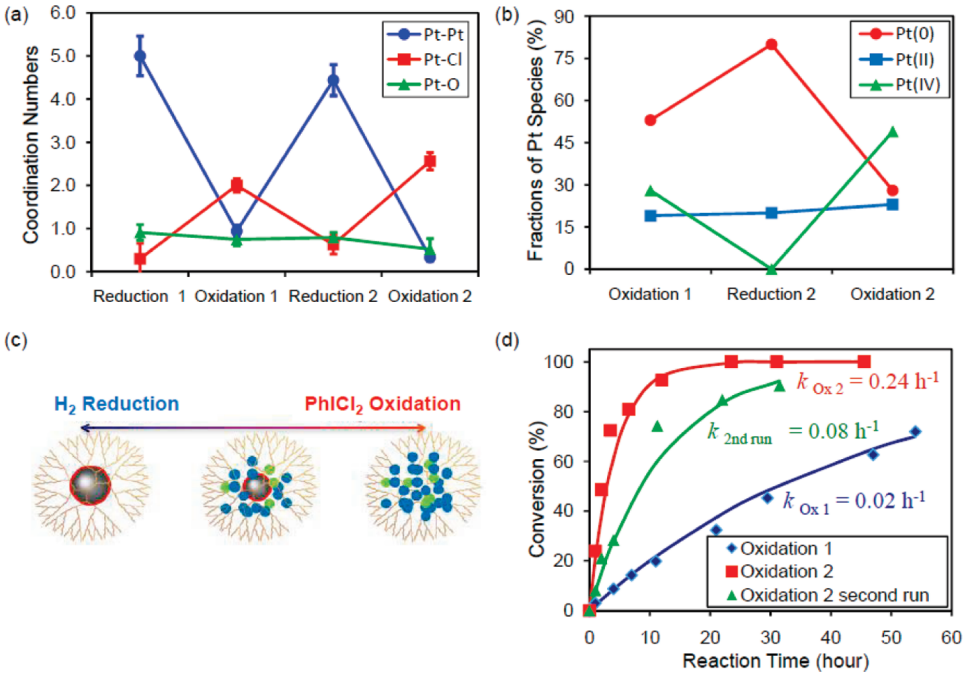

Figure 1. (a) Average coordination numbers of Pt atoms in the supported Pt catalyst after a sequence of hydrogen reduction and $PhICl_2$ oxidation treatments in the toluene derived from EXAFS analysis. (b) The fractions of Pt(0) and Pt(II) and Pt(IV) chloride species of the Pt catalyst derived from NEXAFS analysis. (c) A scheme based on the XAS results, showing possible structures of the dendrimer-encapsulated Pt catalyst after reduction and oxidation treatment. The gray spheres represent the metallic Pt clusters. The surface Pt chlorides are indicated by red circles. The small blue and green species represent the Pt(II) and Pt(IV) species formed after oxidation treatment. (d) The reaction conversions vs reaction time for preoxidized samples with 1 wt % Pt loading: **Oxidation 1** and **Oxidation 2**. The rate constants, k_{ox1} and k_{ox2}, are obtained by fitting the conversions (red ■ and blue ◆) to the kinetic model for unimolecular reaction. The red and blue solid lines are the fitting curves. For **Oxidation 2**, a second run of batch reaction is performed after the first run of reaction reached a full conversion by adding fresh reactant into the reaction mixture. The conversion versus reaction time of the second run is given by green ▲. $k_{\text{second run}}$ is the rate constant of the second run.

a second run of reaction was performed by adding a fresh batch of the reactant (same amount as the first run) into the reaction mixture after the first run reached a full conversion. The conversion versus reaction time of the second run is given by green ▲ in Figure 1d. The apparent rate constant of the second run is about one-third of that of the first run, which indicates a marked deactivation of the catalyst.

To correlate the catalyst deactivation with the changes in the fraction of Pt active species under the reaction conditions, the evolution of the Pt chloride species in the catalyst was monitored by in situ NEXAFS at 100 °C (see Experimental Section for detail). In the in situ experiment, a preoxidized catalyst was used, in which the initial fractions of Pt(0), Pt(II), and Pt(IV) species were about 46%, 26%, and 26%, respectively. Figure 2a shows the evolution of fractions of Pt species as the reaction proceeded. Under the reaction conditions (the solid lines in Figure 2a), a marked decrease of the Pt(IV) fraction occurred within about 2 h after the reaction was initiated. Apparently, the highly electrophilic Pt(IV) species is not stable under the reaction conditions.

On the other hand, the fraction of Pt(II) species (Figure 2a, the solid blue line) rapidly increased as that of the Pt(IV) species decreased while the fraction of Pt(0) did not change significantly, which indicates that most Pt(IV) species are converted to the Pt(II) species. In the steady state of the catalyst composition, the Pt(II) fraction was kept at approximately 42% (Table S3), in which approximately 16% was converted from Pt(IV). The reaction kinetics measurement under the same reaction conditions (Figure 2b) shows that more than 50% of the total product yield was produced after the catalyst reached its steady state. Therefore, the Pt(II) species is quite stable under the reaction conditions.

The in situ NEXAFS studies also shed light on the mechanistic basis of catalyst deactivation. As described above, a marked deactivation of **Oxidation 2** was observed in the second run of the sample (Figure 1d). On the basis of the facts that (1) the Pt(IV) species rapidly converts to the Pt(II) species under reaction conditions, and (2) the Pt(II) species is stable under reaction conditions, the second-run catalyst sample should have a higher fraction of Pt(II) and a lower fraction of Pt(IV), as compared to the as-prepared **Oxidation 2**. Despite the higher fraction of the Pt(II) species in the second-run sample, the rate constant of the second run was only one-third of that of the first run. Therefore, the observed deactivation is mainly caused by the instability of the Pt(IV) species under reaction conditions.

Stability against Leaching. The leaching process in this metal-cluster catalyst may involve the diffusion of Pt ions from inside the dendrimer to the solvent. Figure 1a and b shows that, after the second reduction treatment, **Reduction 2** has an average Pt—Pt coordination number close to 4.5, and the Pt(0) fraction in this sample is about 80%. These observations suggest that, after the reduction of **Oxidation 1**, a large portion of Pt atoms is reduced to form metal clusters. In other words, no significant leaching of the Pt ions from inside the dendrimer occurs during the solution-phase pretreatment to prepare **Oxidation 1**. Otherwise, one would not expect to recover a high fraction of Pt(0) clusters after the reduction.

dx.doi.org/10.1021/ja204191t |*J. Am. Chem. Soc.* 2011, 133, 13527–13533

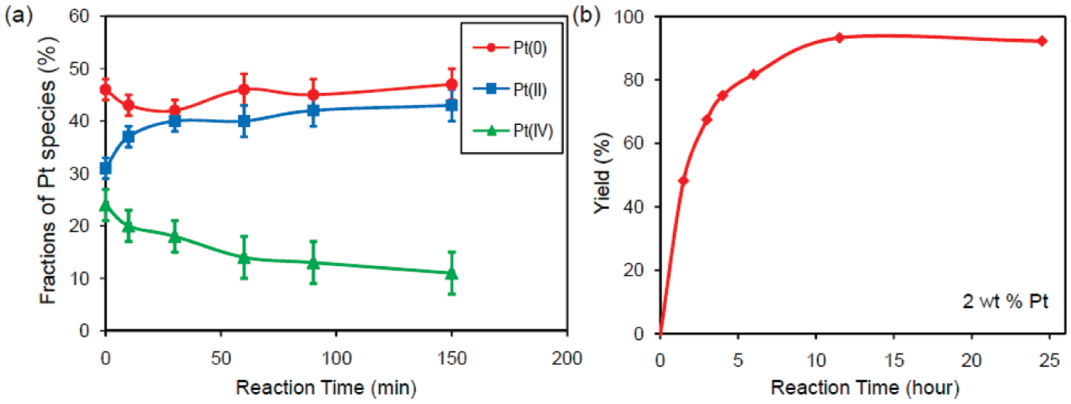

Figure 2. (a) The evolution of Pt species in the supported catalyst obtained by NEXAFS measurements under reaction conditions. The sample, 2 wt % Pt catalyst, was preoxidized by $PhICl_2$. (b) The product yield as a function of time obtained in a batch reaction under identical conditions.

Table 1. Pt Content Loss in the Supported Catalyst and Pt Concentration in the Hydrophilic Solutions after Reaction, Obtained from ICP-MS Measurements[a]

reaction solvent	Pt content loss in the supported catalyst (wt %)	solution Pt concentration (ppm)
dioxane	0.04	41.5
dioxane + 2.5% H_2O	0.10	50.2
dioxane + 5.0% H_2O	0.12	81.0

[a] The Pt content in the unused catalyst is 0.632 wt %.

The EXAFS results in Figure 1a also show that the Pt−O (or N) coordination number is less than 1 for all of the samples, which suggest that a large portion of the Pt atoms in these samples are not covalently bonded to the amino or hydroxyl groups present in the dendrimer. Thus, the covalent bonding between Pt and the reactive sites in the dendrimers is not likely to be the major force keeping the Pt ions from leaching. Other than the diffusion of Pt ions, there is another possible leaching pathway in which metal-containing dendrimers desorb from the surface of silica support into solvent because, in this Pt catalyst, the dendrimers are not covalently bonded to the support surface.

To explain the observed stability against leaching, one may notice that the solvent, toluene, used in this reaction is nonpolar, while the components of the catalyst including the Pt ion, the PAMAM G4-OH dendrimer, and the silica support are polar materials. These polar materials should have a low solubility in the toluene. Thus, as long as this catalyst is used in a nonpolar solvent, the Pt ions would preferentially stay in the polar environment within the dendrimer, and the dendrimers would preferentially anchor on the surface of polar silica support.

To substantiate this hypothesis, water−dioxane mixtures were used as the reaction solvent in a series of control experiments. The ICP-MS elemental analysis data of Pt for content loss in the catalyst and Pt amount in the reaction solution are shown in Table 1. In pure dioxane, a somewhat polar solvent, a small amount of Pt leaching was detected. The addition of a trace amount of water into the reaction mixture resulted in an increase of Pt leaching, accompanied by a significant increase in the conversion rate (Figure 3), which is another indication of the leaching of active Pt species in the solvent. Thus, the disparity in the polarity of the reaction solvent and of the components of the supported Pt catalyst is a crucial factor to keep Pt from leaching in toluene.

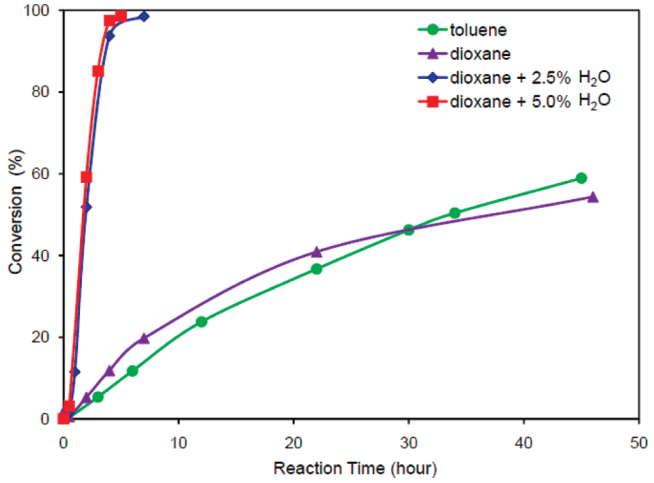

Figure 3. Product yield as a function of reaction time for the reactions where several hydrophilic solvents were used. The Pt loading in the catalyst is 1 wt %.

In water, the leaching of Pd was previously observed by de Jesus and co-workers when a polar-dendrimer-encapsulated Pd cluster catalyst (Pd_{40} G4OH) was used for the Stille reaction at 40 °C.[23] In contrast, the leaching of a silica-supported Pd_{40} G4OH catalyst was inhibited when a π-bond activation reaction was carried out in toluene.[15] Therefore, the polar−nonpolar repulsive interaction between solvent and catalyst materials may provide a general leaching-inhibition mechanism for the solution-phase reactions under mild reaction conditions.

CONCLUSIONS

In this work, XAS studies show that the coordination numbers and oxidation state of Pt in the dendrimer-encapsulated metal clusters can be easily altered by cycles of reduction and oxidation treatment due to the small size (~1 nm) of the metal clusters. After an initial reduction treatment, the Pt−Pt coordination number derived from EXAFS analysis is about 5, which indicates an average particle size of about 1 nm. After a subsequent oxidation treatment by $PhICl_2$, the Pt−Pt coordination number decreases to about 1 and the Pt−Cl coordination number increases to about 2. The second reduction treatment brings the Pt−Pt coordination number back to about 4.5, and the metallic-cluster structure is largely recovered.

After oxidation by $PhICl_2$, the activated Pt catalyst is a mixture of metallic Pt(0) and Pt(II) and Pt(IV) chlorides. The reaction kinetics results show that the conversion rate increases with the fractions of Pt(IV) species in the preoxidized catalyst. Therefore, the Pt(IV) species is more active than the Pt(II) species. The evolution of the fractions of Pt species monitored by in situ XAS measurements further unveils that the Pt(IV) species is not stable under the reaction conditions, and that the Pt(IV) species partially converts to the Pt(II) species as the reaction proceeds. The depletion of the fraction of the Pt(IV) species in catalyst samples correlates with the catalyst deactivation observed in the reaction kinetics study. Stabilizing the highly electrophilic Pt(IV) species under the reaction conditions is crucial for utilizing this catalyst to perform reactions in a continuous flow mode where a long and active lifetime of the catalyst is required.

The aforementioned reversibility of metallic-cluster structure suggests that, after oxidation, Pt ions (Pt(II) and Pt(IV)) can be stabilized inside the dendrimer without leaching into toluene. On the basis of the structural information, we attribute the stability against leaching of this catalytic system to the disparity in the polarity of toluene solvent and of the components in the Pt catalyst. This mechanism of stabilization is supported by a series of control experiments in which the leaching of Pt species is only detectable when several hydrophilic solvents are used.

Furthermore, it is intriguing that the supported Pd catalyst discussed in a previous publication has a catalytic activity even higher than that of most known Pd-based homogeneous catalysts at room temperature.[15] Current findings for the catalytically active Pt species provide important insights into the high activity associated with the Pd catalyst. First, Pd is more electropositive than Pt; therefore, in the same oxidizing environment, the Pd catalyst may be more oxidized than the Pt catalyst.[24] Second, the use of small Pd clusters of 1 nm in size enables the preparation of a highly dispersed metal-ion catalyst inside the dendrimers upon oxidation by $PhICl_2$. The highly dispersed metal-ion catalyst is not affected by the low solubility of Pd ions in toluene, which is known to inhibit the use of metal salts in many homogeneous catalytic processes. A XAS study on the Pd catalyst will be reported in the near future to provide more detailed information.

Finally, on the basis of the studies in this work, we conclude with several guidelines, which may help future design metal-cluster-based catalysts for homogeneous reactions: (1) monodispersed metal cluster <1 nm in size should be considered as a precatalysts so that the chemical state of the catalyst can be effectively tuned by appropriate pretreatment to generate the activated catalysts containing a high fraction of active species; (2) combining ex situ and in situ structure characterization of the catalysts with a comparative reaction kinetic study is invaluable for optimization of catalytic performance by identifying the most active species and stabilizing the active species under the reaction conditions; and (3) stabilizing active species against leaching by the nonpolar−polar repulsion between catalyst materials and reaction solvent should be considered a useful leaching-inhibition mechanism under mild reaction conditions.

EXPERIMENTAL SECTION

Catalyst Preparation. The details of the catalyst preparation have been given in a previous publication.[12,25] Briefly, the Pt clusters were encapsulated by fourth generation polyamidoamine (PAMAM) dendrimers. The clusters were then loaded onto mesoporous silica (SBA-15) to improve the recyclability of the catalyst. The metal loading of the catalyst was controlled by the weight ratio of Pt atoms to the silica support material. The size of the Pt cluster was controlled by the molar ratio of metal ion precursor to dendrimer. The mole ratio of 40:1 was used for all samples in this study. The supported Pt catalyst was then pretreated by reduction under 1 atm of hydrogen at 100 °C for 24 h. The reduced catalyst is referred to as **Reduction 1**. In the oxidation pretreatment, the reduced catalyst was dispersed into toluene, and 3 equiv of $PhICl_2$ per Pt atom was added. The catalyst was oxidized for 45 min at 100 °C. The sequence of oxidation and reduction treatments and the sample codes are given in Scheme 2.

Scheme 2. Sample Treatments and Codes

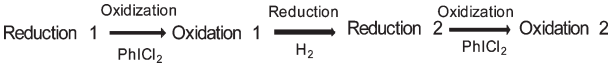

For the ex situ XAS measurements, each pretreated catalyst (**Reduction 1**, **Oxidation 1**, **Reduction 2**, and **Oxidation 2**) was loaded into a quartz capillary tube with toluene under an argon or nitrogen atmosphere, and then the capillary was sealed by epoxy. The capillary was centrifuged, which resulted in the sedimentation of solid catalyst at the bottom of the capillary. The Pt loading in the samples was 5 wt %.

For in situ XAS measurements, a sample with 2 wt % of Pt loading was used. To mimic the reaction condition for reaction kinetics study in the small-volume capillary, it was made sure that the Pt:reactant molar ratio was about 1:30. The concentration of the reactant in toluene is about 0.087 M. In the sample for the reaction with oxidant, 3 equiv of $PhICl_2$ per Pt atom was added in the reaction mixture.

XAS Measurements and Data Analysis. The XAS measurements in this work were performed at beamline 10.3.2 at Advanced Light Source (ALS) at Lawrence Berkeley National laboratory (Berkeley, CA)[26] and beamline 4-1 at Stanford Synchrotron Radiation Lightsource (Menlo Park, CA). The data were collected in fluorescence mode at the Pt L_3 edge (11.564 keV). A bulk Pt foil was measured in transmission mode simultaneously with samples for calibration purposes. For ex situ measurements, all spectra were taken at room temperature. Multiple scans (up to 8) were collected for each sample.

For in situ XAS measurement, the QuickXAS mode at beamline 10.3.2 at ALS was utilized. In this mode, one scan covering the near-edge region (up to 300 eV at the Pt L_3 edge) takes about 3 min. A reactor consisting of a heating block and a quartz capillary tube was built for in situ measurement (Scheme S1 in the Supporting Information). The heating block was preheated to 100 °C, and then the capillary tube loaded with the reaction mixture was dropped into a sample hole in the heating block to initiate the reaction. The X-ray emission from Pt was detected through a hole in the heating block.

For EXAFS analysis, the software at the beamline was used to perform deadtime correction, energy calibration, glitch removal, pre-edge subtraction, postedge normalization, and conversion to *k*-space. The Artemis software from the IFEFFIT package was used to fit the EXAFS signal.[27] The FEFF8.2 code was used to generate theoretical standards.[28] The *k*-range was from 2.0 to 13.5 $Å^{-1}$ and the *R*-range from 1.2 to 3.2 Å, which gave 14 independent data points according to the Nyquist formula. The number of fitting variables was up to 8 in the analysis of all samples. In the EXAFS fits for each sample, three shells (Pt−Pt, Pt−Cl, and Pt−O) were used, and the energy shifts and the mean squared displacements of scatterers were slaved to minimize the error bars of fitting parameters (Table S1). The fitting quality is shown in Figure S1.

EXAFS analysis provides the average coordination numbers of the neighbors surrounding a Pt atom. If Pt atoms are in a uniform chemical environment such as that in the bulk crystalline material, EXAFS results may provide the structural information directly. However, if a sample consists of nanoparticles with a wide size distribution, EXAFS analysis alone is not sufficient to provide the structural information.[29] Therefore,

NEXAFS analysis was performed by fitting a sample spectrum by a linear combination of several standard spectra, which provides the fractions of Pt(0), Pt(II), and Pt(IV) species in the samples. In combination with EXAFS analysis, NEXAFS analysis has enabled us to elucidate the complex structure of our samples.

For NEXAFS analysis, attempts were made to fit the near-edge spectra of our Pt dendrimer sample by a linear combination of standard spectra from Pt foil, $PtCl_2$, $PtCl_4$, and PtO_2 bulk materials. The obtained fits were not good with the *R*-factors in the order of 10^{-4}. It was observed that the EXAFS wiggles on the Pt dendrimer samples are consistently attenuated with respect to those of the fitting spectra. We believe that this is due to significantly fewer nearest and second nearest neighbors of Pt in our small dendrimer nanoparticles as compared to these crystalline standards. To achieve better fitting quality, the spectra of **Reduction 1**, Zeise's Pt dimer ($[\{(\eta^2\text{-}C_2H_4)PtCl_2\}_2]$),[30] K_2PtCl_4, and H_2PtCl_6, were used as standards for the partially oxidized small Pt cluster, $Pt(II)Cl_2$, and $Pt(IV)Cl_4$ species, respectively (Figure S2). The small EXAFS wiggles on these spectrum standards indicate that these standard compounds are not in crystalline form. The use of these standards resulted in good fits with *R*-factor in the order of 10^{-5} for all of the sample spectra as shown in Figure S3 and Table S2.

The use of one of our samples, **Reduction 1**, as a standard can be justified as follows. First, the structure of Pt dendrimer nanoparticles after reduction treatment similar to that undergone by **Reduction 1** has been studied extensively by several research groups.[29,31] The general conclusion is that Pt clusters form after gas-phase reduction by H_2, and that the Pt clusters are partially oxidized with O or N coordinated. The Pt−Pt and Pt−O coordination numbers vary depending on hydrogen pressure, temperature, and time duration of the reduction treatment. Our EXAFS analysis shows that the Pt−Pt and Pt−O or N coordination numbers for **Reduction 1** are about 4.9 and 1.2, respectively. Second, it is the catalytic activity of Pt chloride species that is responsible for the electrophilic catalysis in our system. Note that **Reduction 1** mainly consists of Pt(0) and a small amount of PtO_x, so it is reasonable to investigate the concentration evolution of the Pt chloride species after subsequent treatments by using **Reduction 1** and suitable Pt chlorides as the standards.

NEXAFS Analysis of in Situ XAS Data. For the in situ XAS data presented in Figure 2a, each data point was obtained from an average spectrum of five consecutive scans. The time period for five scans was about 15 min, which is short enough to catch the evolution of Pt species for this reaction. QuickXAS measurement was used to monitor the fractions of Pt species for 15 h after the reaction initiated. The NEXAFS spectra of the catalyst before and after reaction were taken in the reaction mixture and at room temperature. The NEXAFS fitting parameters are shown in Tables S3 and S4. Several NEXAFS fits of in situ data are also shown in Figure S4.

Reaction Kinetics Studies. For monitoring the kinetic behavior of **Oxidation 1** and **Oxidation 2** (Figure 1d), in an oven-dried Schlenk flask equipped with a stopcock side arm was added catalyst (**Oxidation 1** or **Oxidation 2**, contained ∼0.0044 mmol of Pt, ∼3.5 mol % with respect to 2-(phenylethynyl)phenol) in a glovebox. A solution containing 2-(phenylethynyl)phenol (24.3 mg, 0.125 mmol) and hexamethylbenzene (internal standard for GC analysis, 20.3 mg, 0.125 mmol) in 4 mL of toluene was subsequently added the Schlenk flask. The concentration of 2-(phenylethynyl)phenol in the reaction mixture was 0.031 M. The reaction mixture was degassed by three freeze−pump−thaw cycles. The thawed reaction mixture was placed in an oil bath preheated to ∼100 °C and was stirred under a nitrogen atmosphere. The progress of reaction was monitored by GC analysis. A ∼100 mL aliquot was taken at each sampling. Each aliquot was passed through a microfiber filter (Whatman WF/F) and was diluted with 1 mL of EtOAc, before being injected into the GC. In the case where **Oxidation 2** was used, another batch of 2-(phenylethynyl)phenol (24.3 mg, 0.125 mmol) was added to the Schlenk flask ∼31 h after the reaction first began. The reaction was monitored as described above.

For the comparison with in situ XAS results in Figure 2b, the reaction was carried out and monitored following the procedure described above. However, the following stoichiometry and concentration were used: preoxidized catalyst (2 wt % Pt loading, contained ∼0.0062 mmol of Pt, ∼2 mol % with respect to 2-(phenylethynyl)phenol) was mixed with a solution containing 2-(phenylethynyl)phenol (59.7 mg, 0.31 mmol) and hexamethylbenzene (internal standard for GC analysis, 49.9 mg, 0.31 mmol) in 1.5 mL of toluene. The concentration of 2-(phenylethynyl) phenol in the reaction mixture was 0.2 M.

For leaching studies (Figure 3), in an oven-dried Schlenk flask equipped with a stopcock side arm, 1 wt % Pt_{40} G4OH/SBA-15 (contained ∼0.0044 mmol of Pt, ∼3.5 mol % with respect to **1**) was stirred under 1 atm of H_2 in an oil bath preheated to ∼100 °C for 24 h. The heating was then stopped, and all of the H_2 in the system was pumped away under reduced pressure. A solution containing 2-(phenylethynyl)phenol (24.3 mg, 0.125 mmol), $PhICl_2$ (3.6 mg. 0.013 mmol), and hexamethylbenzene (internal standard for GC analysis, 20.3 mg, 0.125 mmol) in 4 mL of specified solvent (toluene or dioxane) and a specified amount of water was subsequently added to the Schlenk flask. The concentration of 2-(phenylethynyl)phenol in the reaction mixture was 0.031 M. The reaction mixture was degassed by three freeze−pump−thaw cycles. The thawed reaction mixture was placed in an oil bath preheated to ∼100 °C and was stirred under a nitrogen atmosphere. The progress of reaction was monitored by GC analysis. A ∼100 μL aliquot was taken at each sampling. Each aliquot was passed through a microfiber filter (Whatman WF/F) and was diluted with 1 mL of EtOAc, before injection into the GC.

■ ASSOCIATED CONTENT

Supporting Information. Illustration of the in situ XAS cell (Scheme S1), tabulated fitting parameters for ex situ and in situ XAS data (Tables S1−S3), and EXAFS and NEXAFS spectra and representative fits (Figures S1−S4). This material is available free of charge via the Internet at http://pubs.acs.org.

■ AUTHOR INFORMATION

Corresponding Author
somorjai@berkeley.edu; fdtoste@berkeley.edu

Author Contributions
†These authors contributed equally.

■ ACKNOWLEDGMENT

We acknowledge support from the Director, Office of Science, Office of Basic Energy Sciences, Division of Chemical Sciences, Geological and Biosciences of the U.S. DOE under Contract No. DE-AC02-05CH11231.

■ REFERENCES

(1) Gladysz, J. A. *Chem. Rev.* **2002**, *102*, 3215–3216.
(2) Beach, E. S.; Cui, Z.; Anastas, P. T. *Energy Environ. Sci.* **2009**, *2*, 1038–1049.
(3) Astruc, D.; Lu, F.; Aranzaes, J. R. *Angew. Chem., Int. Ed.* **2005**, *44*, 7852–7872.
(4) Jones, C. W. *Top. Catal.* **2010**, *53*, 942–952.
(5) Buchmeiser, M. R. *Chem. Rev.* **2008**, *109*, 303–321.
(6) van Heerbeek, R.; Kamer, P. C. J.; van Leeuwen, P.; Reek, J. N. H. *Chem. Rev.* **2002**, *102*, 3717–3756.
(7) Grubbs, R. B. *Polym. Rev.* **2007**, *47*, 197–215.

(8) Astruc, D. *Tetrahedron: Asymmetry* **2010**, *21*, 1041–1054.
(9) Reimann, S.; Stotzel, J.; Frahm, R.; Kleist, W.; Grunwaldt, J.-D.; Baiker, A. *J. Am. Chem. Soc.* **2011**, *133*, 3921–3930.
(10) Phan, N. T. S.; Van Der Sluys, M.; Jones, C. W. *Adv. Synth. Catal.* **2006**, *348*, 609–679.
(11) Astruc, D.; Boisselier, E.; Ornelas, C. *Chem. Rev.* **2010**, *110*, 1857–1959.
(12) Witham, C. A.; Huang, W. Y.; Tsung, C. K.; Kuhn, J. N.; Somorjai, G. A.; Toste, F. D. *Nat. Chem.* **2010**, *2*, 36–41.
(13) Fürstner, A. *Chem. Soc. Rev.* **2009**, *38*, 3208–3221.
(14) Fürstner, A.; Davies, P. W. *J. Am. Chem. Soc.* **2005**, *127*, 15024–15025.
(15) Huang, W. Y.; Liu, J. H.-C.; Alayoglu, P.; Li, Y. M.; Witham, C. A.; Tsung, C. K.; Toste, F. D.; Somorjai, G. A. *J. Am. Chem. Soc.* **2010**, *132*, 16771–16773.
(16) Evans, J.; O'Neill, L.; Kambhampati, V. L.; Rayner, G.; Turin, S.; Genge, A.; Dent, A. J.; Neisius, T. *J. Chem. Soc., Dalton Trans.* **2002**, 2207–2212.
(17) Somorjai, G. A.; Li, Y. M. *Top. Catal.* **2010**, *53*, 832–847.
(18) Rohr, M.; Grunwaldt, J.-D.; Baiker, A. *J. Mol. Catal. A: Chem.* **2005**, *226*, 253–257.
(19) Benfield, R. E. *J. Chem. Soc., Faraday Trans.* **1992**, *88*, 1107–1110.
(20) Grass, M. E.; Zhang, Y. W.; Butcher, D. R.; Park, J. Y.; Li, Y. M.; Bluhm, H.; Bratlie, K. M.; Zhang, T. F.; Somorjai, G. A. *Angew. Chem., Int. Ed.* **2008**, *47*, 8893–8896.
(21) Tao, F.; Dag, S.; Wang, L. W.; Liu, Z.; Butcher, D. R.; Salmeron, M.; Somorjai, G. A. *Nano Lett.* **2009**, *9*, 2167–2171.
(22) Pastine, S. J.; Youn, S. W.; Sames, D. *Org. Lett.* **2003**, *5*, 1055–1058.
(23) Bernechea, M.; de Jesus, E.; Lopez-Mardomingo, C.; Terreros, P. *Inorg. Chem.* **2009**, *48*, 4491–4496.
(24) Atkins, R. H. *Trans. Faraday Soc.* **1930**, *26*, 490–496.
(25) Huang, W.; Kuhn, J. N.; Tsung, C. K.; Zhang, Y.; Habas, S. E.; Yang, P.; Somorjai, G. A. *Nano Lett.* **2008**, *8*, 2027–2034.
(26) Marcus, M. A.; MacDowell, A. A.; Celestre, R.; Manceau, A.; Miller, T.; Padmore, H. A.; Sublett, R. E. *J. Synchrotron Radiat.* **2004**, *11*, 239–247.
(27) Ravel, B.; Newville, M. *J. Synchrotron Radiat.* **2005**, *12*, 537–541.
(28) Newville, M.; Ravel, B.; Haskel, D.; Rehr, J. J.; Stern, E. A.; Yacoby, Y. *Physica B* **1995**, *208*, 154–156.
(29) (a) Knecht, M. R.; Weir, M. G.; Myers, V. S.; Pyrz, W. D.; Ye, H. C.; Petkov, V.; Buttrey, D. J.; Frenkel, A. I.; Crooks, R. M. *Chem. Mater.* **2008**, *20*, 5218–5228. (b) Myers, V. S.; Weir, M. G.; Carino, E. V.; Yancey, D. F.; Pande, S.; Crooks, R. M. *Chem. Sci.* **2011**, DOI: 10.1039/c1sc00256b.
(30) Boag, N. M.; Ravetz, M. S. *Acta Crystallogr., Sect. E* **2007**, *63*, M3103–U2208.
(31) Alexeev, O. S.; Siani, A.; Lafaye, G.; Williams, C. T.; Ploehn, H. J.; Amiridis, M. D. *J. Phys. Chem. B* **2006**, *110*, 24903–24914.